PNAS
www.pnas.org

Supplementary Information for

Universal relation with regime transition for sediment transport in fine-grained rivers

Hongbo Ma[a,1], Jeffrey A. Nittrouer[a,1], Baosheng Wu[b], Michael P. Lamb[c], Yuanfeng Zhang[d], David Mohrig[e], Xudong Fu[b, 1], Kensuke Naito[f], Yuanjian Wang[c], Andrew J. Moodie[a], Guangqian Wang[b], Chunhong Hu[g], Gary Parker[f, h,1]

Affiliations:

[a]Department of Earth, Environmental and Planetary Sciences, Rice University, Houston, Texas 77251, USA
[b]State Key Laboratory of Hydroscience and Engineering, Tsinghua University, Beijing 100084, China
[c]Division of Geological and Planetary Sciences, California Institute of Technology, Pasadena, California 91125, USA
[d]Yellow River Institute of Hydraulic Research, Zhengzhou, Henan 450000, China
[e]Jackson School of Geosciences, the University of Texas at Austin, Austin, Texas 78705, USA
[f]Centro de Investigación y Tecnología del Agua, Universidad de Ingeniería y Tecnología, Barranco 15063, Lima, Peru
[g]State Key Laboratory of Simulation and Regulation of Water Cycle in River Basin, Institute of Water Resources and Hydropower Research (IWHR), Beijing 100038, China
[h]Department of Civil and Environmental Engineering, Ven Te Chow Hydrosystems Laboratory, University of Illinois at Urbana-Champaign, Illinois 61801, USA
[i]Department of Geology, University of Illinois at Urbana-Champaign, Illinois 61801, USA

Paste corresponding author name here
Email: H.M., sediment@rice.edu; J.A.N., nittrouer@rice.edu; X.F., xdfu@tsinghua.edu.cn; G.P., parkerg@illinois.edu

This PDF file includes:

Other supplementary materials for this manuscript include the following:

Movies S1

www.pnas.org/cgi/doi/10.1073/pnas.1911225116

Supplementary Information Text

Text S1: Performances of other sediment transport formulae.

Numerous formulae have been developed for fine-grained sediment transport systems where the primary transport mode is suspended load. Previous empirical methods have yielded results that were highly case- and scale- dependent (1, 2). In this regard, much effort has been expended to develop physically-based frameworks satisfying scale independence. In these methods, bedload and suspended load are often treated separately with bedload being the bottom boundary condition for suspended load (3, 4). However, constraining bedload alone is challenging (5-12) and moreover, the linkage between bedload and suspended load has not been fully addressed (13-16). To avoid this issue, bottom boundary conditions for suspended load, independent of bedload, have been proposed (17, 18) for sand-bed rivers; however, their extension to rivers with bed sediment that is a mixture of sand and silt remains problematic. As shown in Table S3, we test UEH and several other representative formulae against our database. We show that UEH represents the best effort so far. It is nonetheless worth exploring problems associated with previous efforts. In the following, we focus on two popular formulae.

To our knowledge, the Laursen (1958) formulation (19) was the first attempt to predict sediment transport rates covering the same wide range of grain sizes discussed herein. The work of van Rijn (1984) represents one of the earliest efforts to systematically construct a complete theoretical framework for sediment transport (both bedload and suspended load), and remains one of the well accepted formulations used in fine-grained systems, including the range of grain sizes covered here (4). Here we study the original form of the van Rijn (1984) formulation. The modified one (20), although adding a correction term for silt-rich environments, neither provides more physical insight nor performs better than the original formulation. At the time of development, the Laursen (1958) formulation consisted of only a graphical curve (19); Brownlie and Brooks (1983) fitted the curve to the piecewise polynomial equation used herein (2).

As outlined in Fig. 3, Table S3 and Fig. S6, we show that the sediment transport predictive capability of UEH outperforms all other formulae including Laursen (1958) and van Rijn (1984) (4, 19), some deficiencies of which have been previously illustrated (2, 21, 22). The relation of van Rijn can well constrain medium and coarse sand transport, but performs poorly with silt and fine sand, as indicated by analyses of both flume and field data (Fig. S6 *A* and *B*). Laursen, on the other hand, underestimates both fine-grained and coarse-grained sediment flux in rivers by an order of magnitude, while being partially supported by flume data (Fig. S6 *C* and *D*). This is likely because the model was developed with, and thus calibrated by, flume data (2, 19). Neither formulation agrees with the data across the full range of system scales. Related problems frequently occur in other formulae as well (2, 21, 22). The strong agreement between UEH and measurements confirm its ability to predict fine-grained sediment transport over a range of hydraulic conditions and bed grain sizes (Table S3; Fig. 3 *A* and *B*). Therefore, UEH stands the universality test and, to our knowledge, is the only formulation that can be expected to perform accurately over both natural and experimental settings possessing fine-grain beds with median bed sediment size spanning two orders of magnitude (11 μm – 1080 μm). Using all the data, we update the parameters for the two regimes of UEH,

$$(\alpha, n) = \begin{cases} (\alpha, n)_{\mathrm{EH}} = (0.046,\ 2.85) \pm (0.0025,\ 0.08) & when \quad Z_{eff} < Z_{eff,c} \\ (\alpha, n)_{\mathrm{GEH}} = (0.96,\ 1.73) \pm (0.09,\ 0.08) & when \quad Z_{eff} \geq Z_{eff,c} \end{cases},$$

where the second parentheses represent the 95% confidence intervals for the parameters. The predictive capacity of the updated UEH does not change much (Table S3).

In addition to the formulae outlined in Table S4 and the dimensionless numbers used therein, we tested a wide range of other dimensionless numbers as well, including Rouse number, effective skin friction Rouse number, Wilcock number (23), etc., and combinations of these parameters. Their predictive capacities were all found to be poorer than UEH.

Text S2: Original and Generalized Engelund-Hansen Theory.

Engelund and Hansen (1967) proposed a bed material load formulation based on a semi-theoretical framework with parameters calibrated by experimental data, by considering energy

conservation for a unit fluid column of sediment-laden flow (24), which moves along the stoss face of a bedform. The energy needed to elevate the column (per unit time) from trough to crest of the bedform is: $\rho RgCHUH_b / L_b$, where *C* is the volumetric average concentration, and H_b and L_b are wave height and wavelength of the bedforms, respectively. The driving power is related to the product of the sediment driving force, $\tau_{sf} - \tau_c$, and bed shear velocity, $u^* = \sqrt{\tau / \rho}$, where τ_{sf} is the bed shear stress due to skin friction, τ_{fd} is bed shear stress due to (bedform) form drag, τ_c is critical shear stress, and $\tau = \tau_{sf} + \tau_{fd}$. Additionally, the total shear stress is $\tau = \rho gHS = \rho C_f U^2$ in steady and uniform flow. In regard to the two types of bed stress, skin friction stress drives sediment transport whereas form drag stress represents resistance to flow produced by topographic irregularities of the channel, and is considered to contribute little to sediment transport. Energy conservation thus dictates that $\rho Rgq_s H_b / L_b = e\left(\tau_{sf} - \tau_c\right)u^*$, where *e* is an efficiency parameter.

Non-dimensionalizing to the respective Einstein and Shields numbers, $q_s^* = q_s / \sqrt{RgD_g^3}$ and $\tau^* = \tau / \left(R\rho gD_g\right)$, we obtain $C_f q_s^* = eC_f L_b / H_b \times \left(\tau_{sf}^* - \tau_c^*\right)\sqrt{\tau^*}$, which is an energy conservation equation without any external assumption. EH found that $C_f L_b / H_b$ takes the constant value 0.235 by means of analysis of data from flume experiments. They similarly found that the relation between skin friction shear stress and total shear stress (in terms of the corresponding Shields numbers) is $\tau_{sf}^* - \tau_c^* = 0.4\tau^{*2}$ for a dune-covered bed. Calibration with flume data yielded *e* = 0.532, giving the original EH relation: $C_f q_s^* = 0.05\tau^{*2.5}$ i.e. (α, *n*) = (0.05, 5/2) with 95% confidence intervals {[0.035, 0.051], [2.50, 2.70]}). Ma et al. (2017) generalized the EH theory (25) by using a general form of the resistance relation: $\tau_{sf}^* - \tau_c^* = b\tau^{*n-0.5}$ and $\alpha = ebC_f L_b / H_b$. Substituting these into the dimensionless energy conservation equation, they obtained the general form of the EH theory: $C_f q_s^* = \alpha\tau^{*n}$. Both parameters *α* and *n* have physical meanings: *α* is proportional to the aspect ratio of the bedforms, and *n* corresponds to the bed state, such that *n* ≥2.0, *n* = 1.5, and *n* < 1.5, represent the conditions of dunes, upper plane bed, and antidunes, respectively. Ma et al. (2017) showed that for fine-grained rivers, (α, *n*) = (0.9, 5/3) with 95% confidence intervals {[0.79, 1.01], [1.58, 1.77]}) (25). This generalized EH formulation (GEH) was calibrated using only one field sediment database measured in the Yellow River, China.

Text S3: Discontinuous jump of sediment load.

According to the UEH formulation, the discontinuity at the regime transition point can be predicted in a theoretical way. To demonstrate this point, we reorganize the UEH formulation into a dimensional form, using independent physical variables only, i.e. GEH: $q_{s,G} = 0.9\frac{1}{C_f}u^{*10/3}R^{-7/6}g^{-7/6}D^{-1/6}$, and EH: $q_{s,O} = 0.05\frac{1}{C_f}u^{*5}R^{-2}g^{-2}D^{-1}$.

Since the regime transition can be driven by even rather modest changes in grain size, we can assume that all hydraulic parameters and grain size are roughly the same, and examine the sediment load ratio of GEH to EH,

$$R_J = \max\left(\frac{q_{s,G}}{q_{s,O}},1\right) = \max\left[18\left(\tau^*\right)^{-5/6},1\right] = \max\left[18\frac{\left(RgD\right)^{5/6}}{u^{*5/3}},1\right].$$

The jump ratio R_J decays as the shear velocity increases, until two regimes merge into one. The relation between R_J and shear velocity, along with relevant verifications, are shown in Fig. S2*A*. Natural flow conditions span a large range of shear velocities, which corresponds to a range of jump ratios. Identification of such a sediment transport regime transition in the fluvio-coastal setting may be particularly significant, because the jump ratio of sediment load can be as much as

one to two orders of magnitude (Fig. S2*A*). Furthermore, for very energetic flow conditions (τ^*>32), two regimes merge into one, which is here assumed to be the GEH regime of UEH instead of EH. It is worth noting that transport of medium-coarse sand material in highly energetic environments (τ^*>>32) has not been fully explored. A natural analogy would be to see how silt and very fine sand react to less strongly energetic flow (τ^*<32), which is the GEH regime of UEH. Thus, we speculate that the transport law for medium-coarse sand is much more likely to be GEH than EH in highly energetic environments (τ^*>>32). A null hypothesis that the sediment transport law corresponds to the EH formula could overestimate the sediment load greatly in the range τ^*>>32.

Table S1. Summary of the hydraulic and grain size characteristics of the sediment data base. U (m/s) is the depth-average flow velocity; H (m) is water depth; S ($\times 10^{-4}$) is channel slope; D_{50} (mm) is the bed material median grain size; C_v ($\times 10^{-4}$) is the volumetric concentration of the bed material sediment, which is comprised of both bedload and a fraction of the bed sediment moving in suspension. *Uncertain field data: outliers from the field data, such that all but these outliers fall within the same regime. Besides unavoidable measurement error, the uncertainties usually come from (1) the ill-defined cutoff grain size for wash load, and (2) unclear transport states (equilibrium or non-equilibrium), neither of which pertains to laboratory flume experiments.

	Regime	**NO.**	***U* (m/s)**	***H* (m)**	***S* ($\times 10^{-4}$)**	**D_{50} (mm)**	**C_v ($\times 10^{-4}$)**
Lab:	GEH	121	0.24 - 1.55	0.094 - 0.37	2.3 - 129	0.011 - 0.153	18 - 865
	EH	690	0.21 - 1.90	0.023 - 0.42	1.1 - 193	0.088 - 1.04	7.55×10^{-4} - 195
Field:	GEH	324	0.379 - 2.896	0.550 - 7.8	0.2 - 6.2	0.020 - 0.158	1.25 - 305
	EH	397	0.206 - 2.270	0.253-14.966	0.021- 15	0.083 – 1.08	2.28×10^{-4} - 15
	UN*	62	0.198 - 2.844	0.79-13.289	0.03 - 9	0.044 - 0.92	6.28×10^{-4} - 237

Table S2. Dimensionless numbers tested for regime diagram.

Dimensionless Numbers	Definition	Note
Dimensionless grain size (D^*)	$D^*=D_g(Rg/v^2)^{1/3}$	First order
Suspension number	u^*/v_s	First order
Gradation coefficient (σ_D)	$\sigma_D=(D_{84}/D_{16})^2$	Second order
Relative roughness	D_{50}/H, D_{90}/H, $3D_{90}/H$, etc.	N/A
Particle Reynolds Number (Re_p)	$Re_p=(RgD_g)^{0.5}D_g/\nu$	N/A
Shear Particle Reynolds Number (Re_P^*)	$Re_p^*=u^*D_g/\nu$	N/A
Reynolds Number (Re)	$Re=4UR_h/\nu$	N/A; R_h hydraulic radius
Shields Number (τ^*)	$\tau^*=\tau/(\rho RgD_g)$	N/A
Dimensionless Skin Friction (τ_{sf}^*)	$\tau_{sf}^*=\tau_{sf}/(\rho RgD_g)$	N/A
Froude Number (Fr)	$Fr=U/\sqrt{gH}$	N/A
Ratio of Channel Width to Depth	W/H	N/A
Yalin Number	$Re_P^*(\tau^*)^{0.5}$	N/A
Fraction of sediment finer than a critical grain size		N/A

Table S3. Comparisons between computed and measured sediment discharge. The present UEH formula and five other widely used formulae are tested against the database. Discrepancy Ratio $DR = Q_{s,c} / Q_{s,m}$ i.e. the ratio of computed sediment discharge to the measured sediment discharge. *Ra* is the average value of *DR* (the closer to unity, the better). MNE (%) = Mean normalized error, $MNE = \frac{1}{N}\sum_{i=1}^{N}\left|\frac{Q_{s,c} - Q_{s,m}}{Q_{s,m}}\right|$ (the closer to zero, the better). AGD = Average geometric deviation, $AGD = \left[\prod_{i=1}^{N} \max\left(Q_{s,c} / Q_{s,m}, Q_{s,m} / Q_{s,c}\right)\right]^{1/N}$ (the closer to unity, the better)

	Flume Experiment						**Field Data**					
Transport mode	High efficiency (GEH)			Low efficiency (EH)			High efficiency (GEH)			Low efficiency (EH)		
Method	*Ra*	*MNE*	*AGD*	*Ra*	*MNE*	*AGD*	*Ra*	*MNE*	*AGD*	*Ra*	*MNE*	*AGD*
UEH	0.87	39.99	1.57	1.42	219.12	1.95	0.91	50.51	1.66	0.80	78.17	2.03
Updated UEH	0.98	45.96	1.59	1.19	131.23	1.86	1.01	56.00	1.66	0.73	82.85	2.22
Laursen (1958)	0.74	88.97	2.18	0.90	134.34	2.04	0.37	59.69	2.98	0.12	84.92	8.60
van Rijn (1984)	0.08	82.96	12.29	1.32	202.25	2.13	0.32	58.70	3.27	0.73	78.35	2.14
Garcia & Parker (1991)	1.2	417	3.94	0.97	144.3	2.36	8.5	2018	10.2	1.86	731	3.95
Wright & Parker (2004)	0.72	416	3.92	0.83	281.5	2.57	0.22	197.0	9.4	0.16	112.9	7.48
van Rijn (2007)	0.12	79.07	8.45	1.32	55.18	2.06	0.36	57.97	3.11	0.73	78.35	2.14

Table S4. Summary of the hydraulic and grain size characteristics of the sediment transport database at Huanyuankou, Yellow River, China. *U* (m/s) is flow velocity; *H* (m) is water depth; S ($\times 10^{-4}$) is channel slope; D_g (mm) is the geometric mean grain size of the bed material; C_v ($\times 10^{-4}$) is the volumetric concentration of the bed material sediment load.

Phase	NO.	*U* (m/s)	*H* (m)	*S* ($\times 10^{-4}$)	D_g (mm)	C_v ($\times 10^{-4}$)	Sampling Dates
Pre-dam (GEH)	82	0.84-2.66	0.77-2.53	0.8-9	0.030-0.158	4.5-408	1980-1990
Post-dam (EH)	19	0.49-2.27	0.59-3.76	0.71-6.7	0.194-0.400	0.078-317	1961-1967 2001-2002

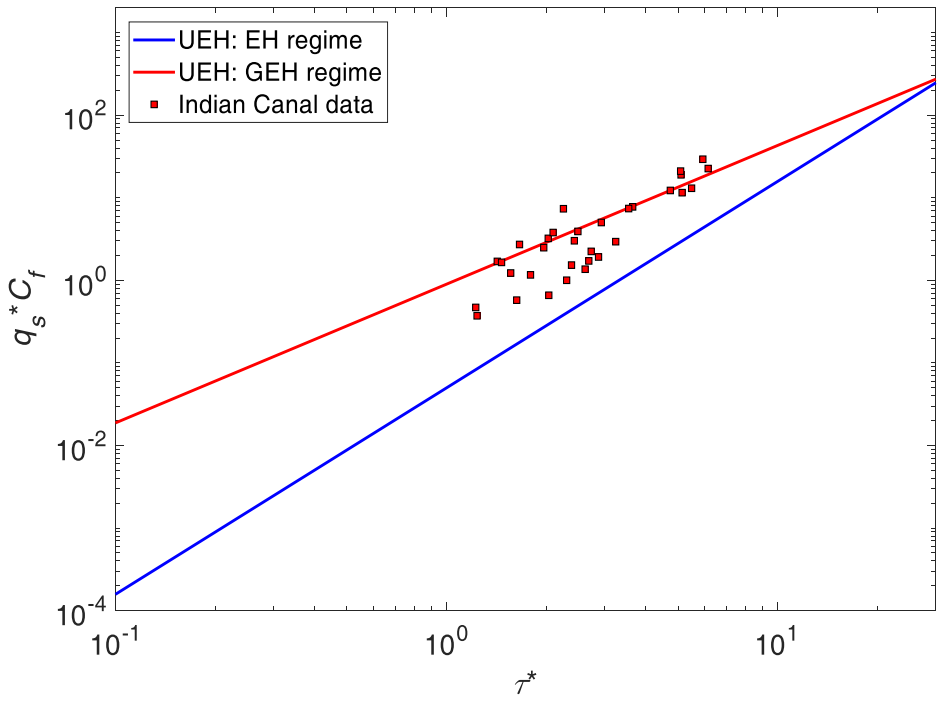

Fig. S1. A field scale sediment transport dataset from Indian Canal (Chitales, 1966) shows similar high transport efficiency behavior as the Yellow River.

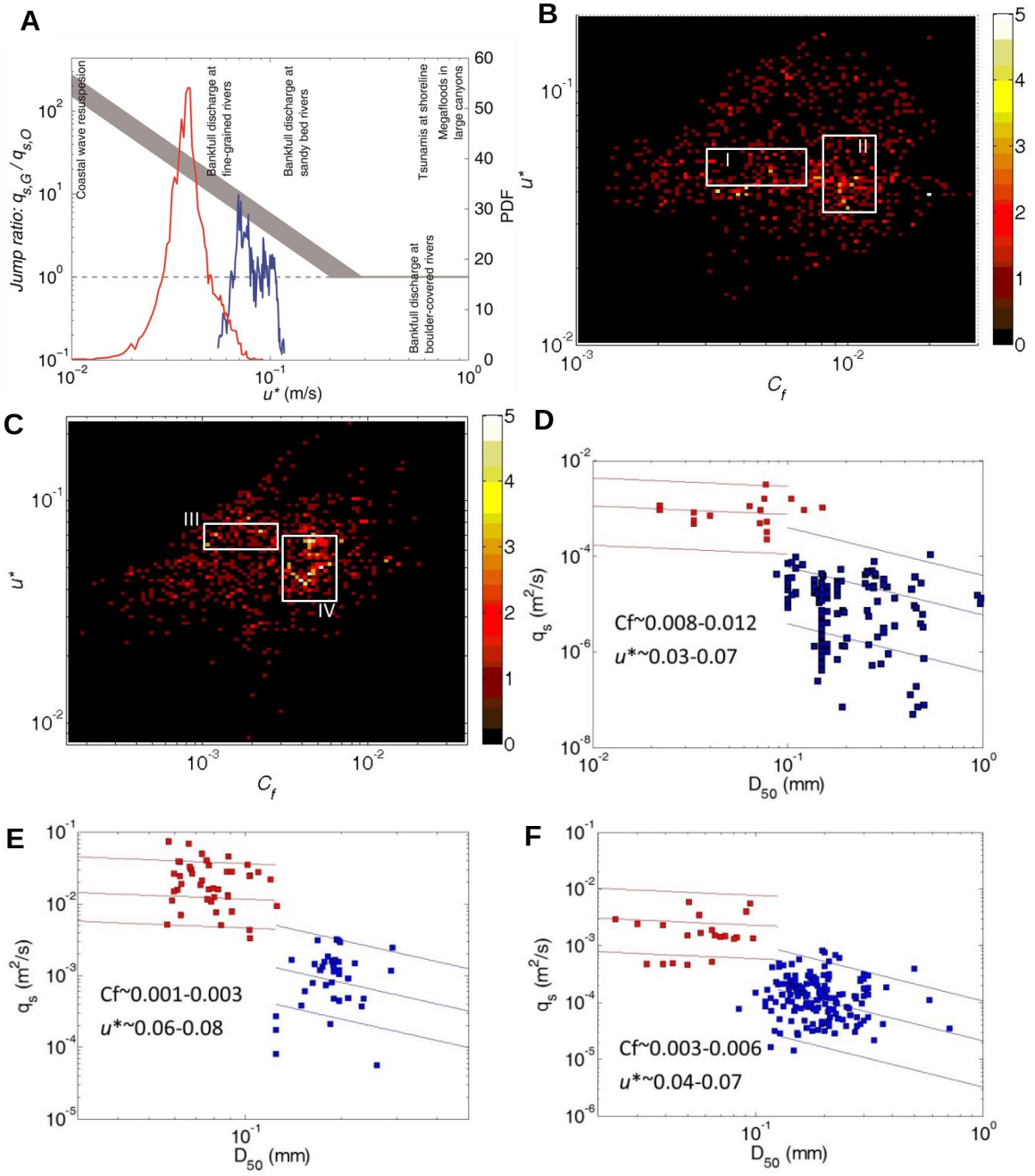

Fig. S2. Discontinuous jump in sediment load. (*A*) Jump ratio $q_{s,G}/q_{s,O}$ decreases as the shear velocity increases until the two regimes merge into one. The red and blue curves are shear velocity distribution (PDF) of the Yellow River, China and the Mississippi River, USA, respectively. Both curves are based on daily discharge measurements. (*B*) Distribution of laboratory data samples in the parameter space (u^*, C_f) and data samples used to show the discontinuity. The brightness indicates the density of data in the parameter space. Data samples from Rectangle I are used for Fig. 1*C*. (*C*) Distribution of field data samples in parameter space and data samples used to show the discontinuity. Rectangles (parameter space), representing various combinations of hydraulic factors, can be arbitrarily chosen to show the discontinuity. The four rectangles are chosen here because they have sufficiently dense data at the transitional

grain size range to show the discontinuity. (*D*) Discontinuous relation between sediment load and grain size based on the laboratory data in Rectangle II of parameter space in (b). (*E*) Discontinuous relation between sediment load and grain size based on the field data in Rectangle III of parameter space in (*C*). (*F*) Discontinuous relation between sediment load and grain size based on the field data in Rectangle IV of parameter space in (*C*).

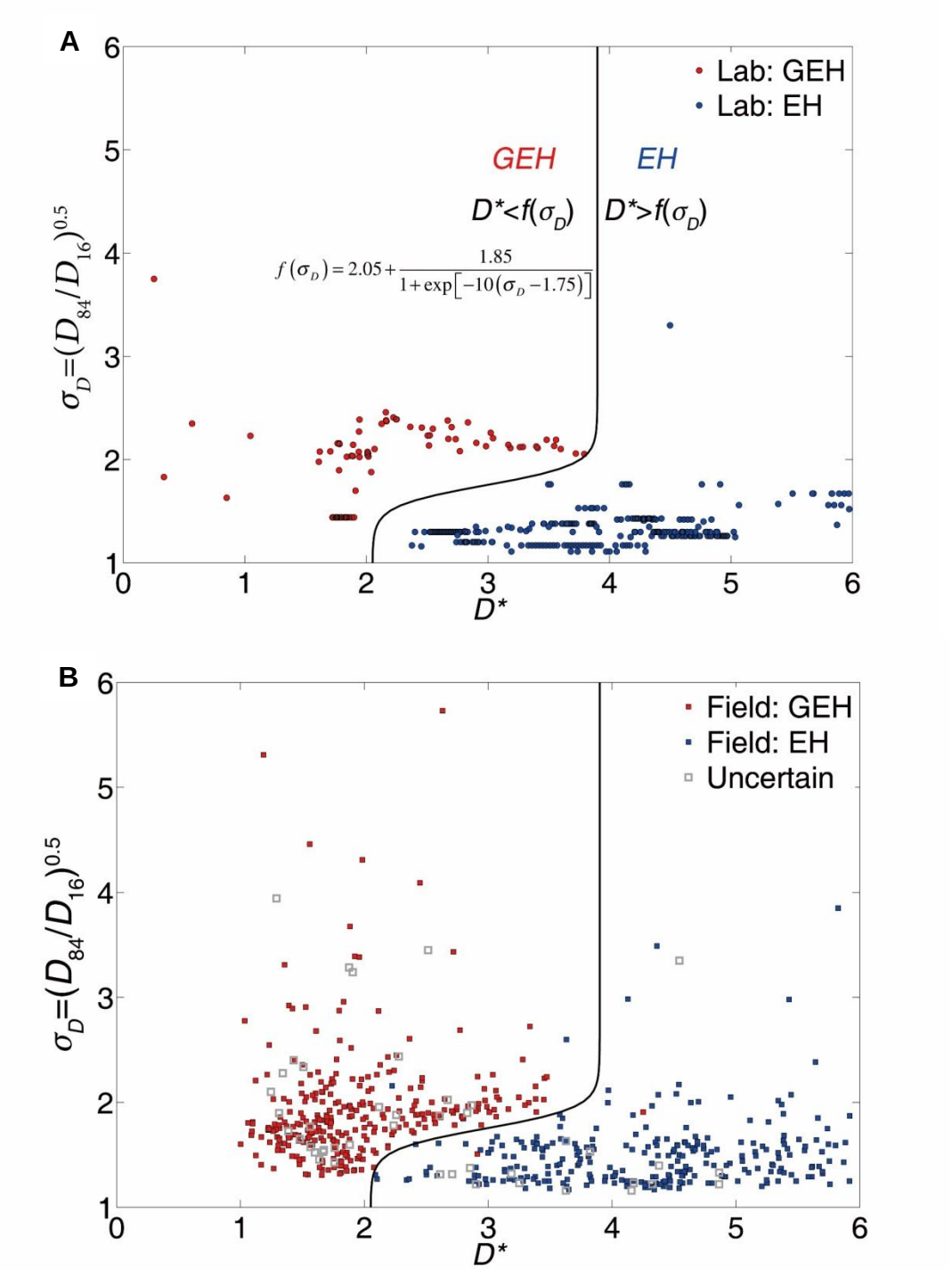

Fig. S3. Regime diagram using the median dimensionless grain size and the graduation coefficient (geometric standard deviation of the grain size) as discriminators. (*A*) Regime diagram against laboratory data. (*B*) The same regime diagram in a tested against field data. The field data agree with the regime diagram developed from laboratory data in (*A*). A small portion of field data was found to be of uncertain regime state. These data are the outliers, such that all but these outliers fall within the same regime (Table S1).

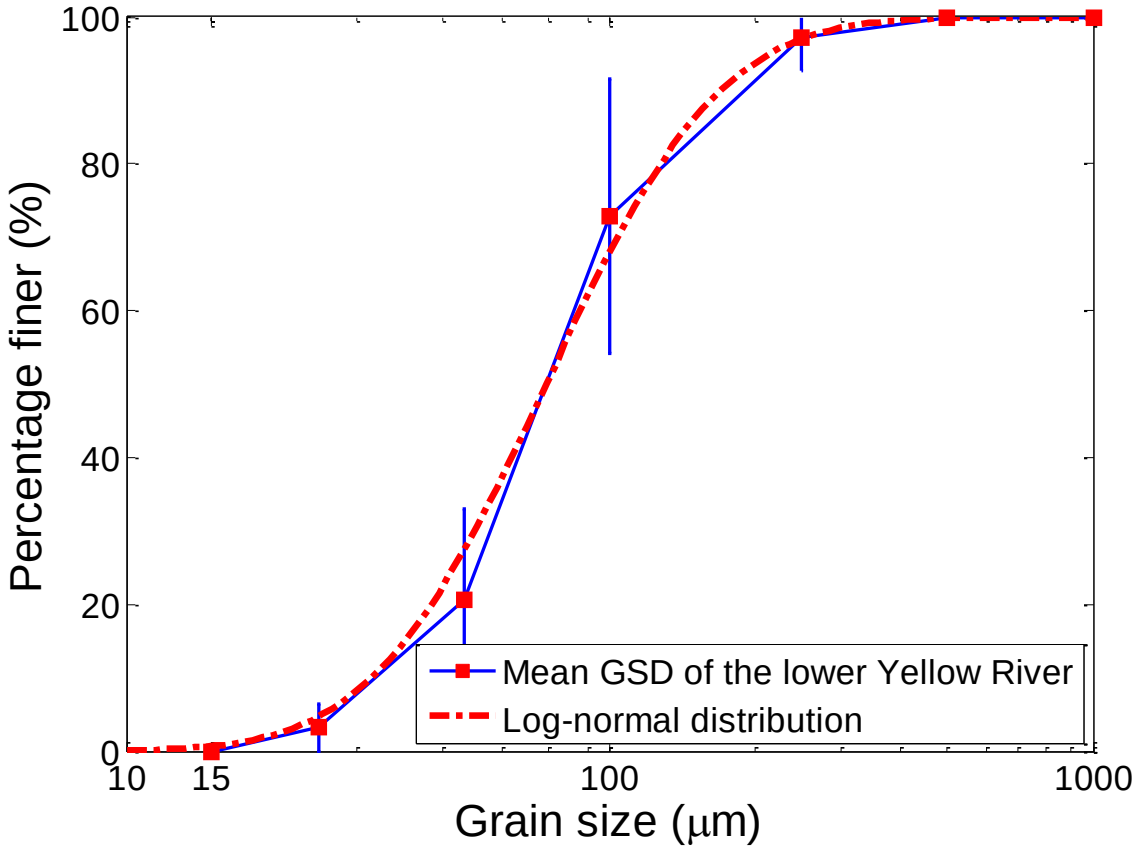

Fig. S4. Grain size distribution (GSD) of the normalized bed material from the lower Yellow River versus the log-normal distribution function. The mean normalized GSD of the bed material of the lower Yellow River has D_{50} = 73.9 μm and σ_D = 1.91, and the same parameters are used for the log-normal distribution. It was found in the lower Yellow River D_5 = 15 μm is an appropriate cut-off grain size for separating the bed material load and wash load (25). In this paper, the same cut-off criterion is used to normalize the bed material of the lower Yellow River.

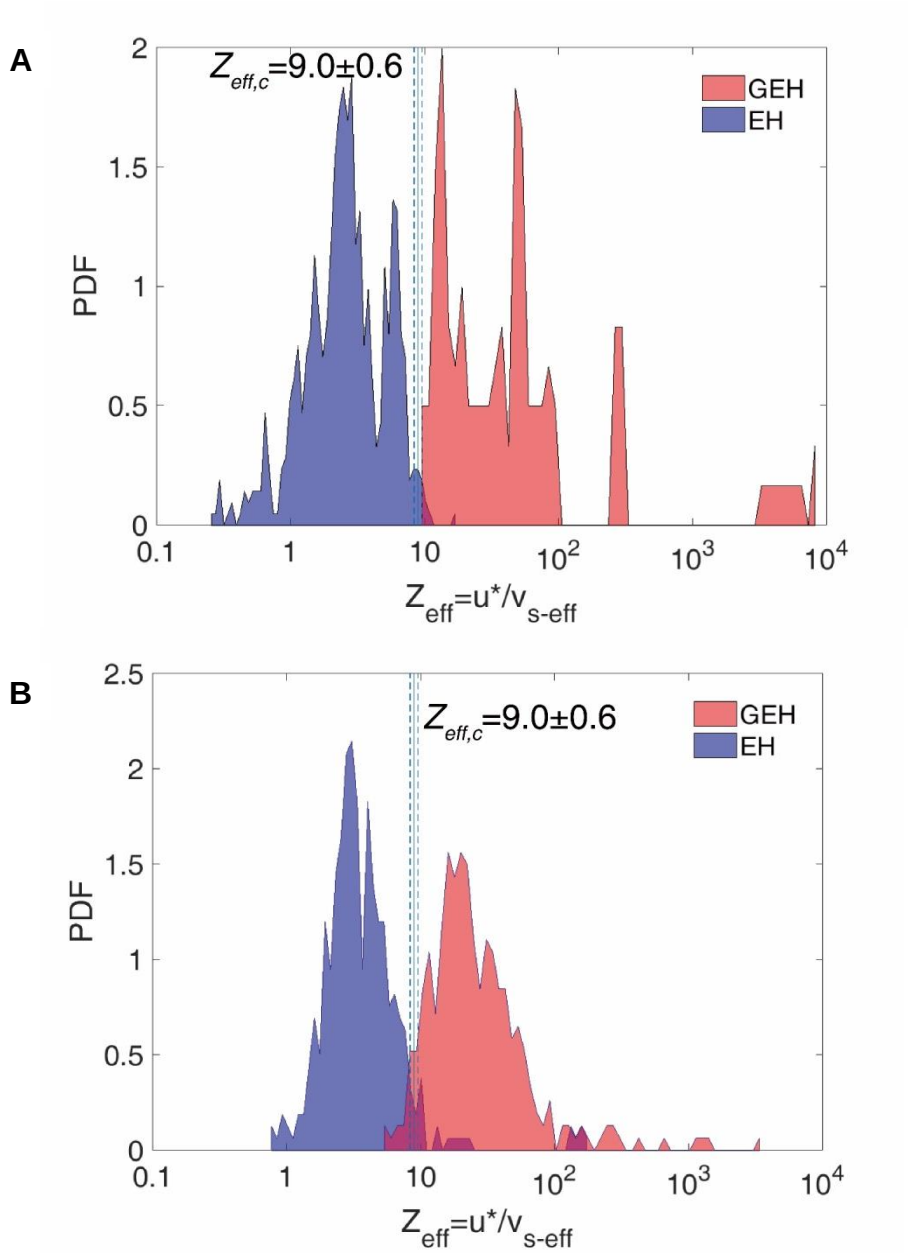

Fig. S5. PDF of the effective suspension number from both the laboratory (*A*) and field data (*B*). The same critical suspension number used as the regime demarcation works for both sets.

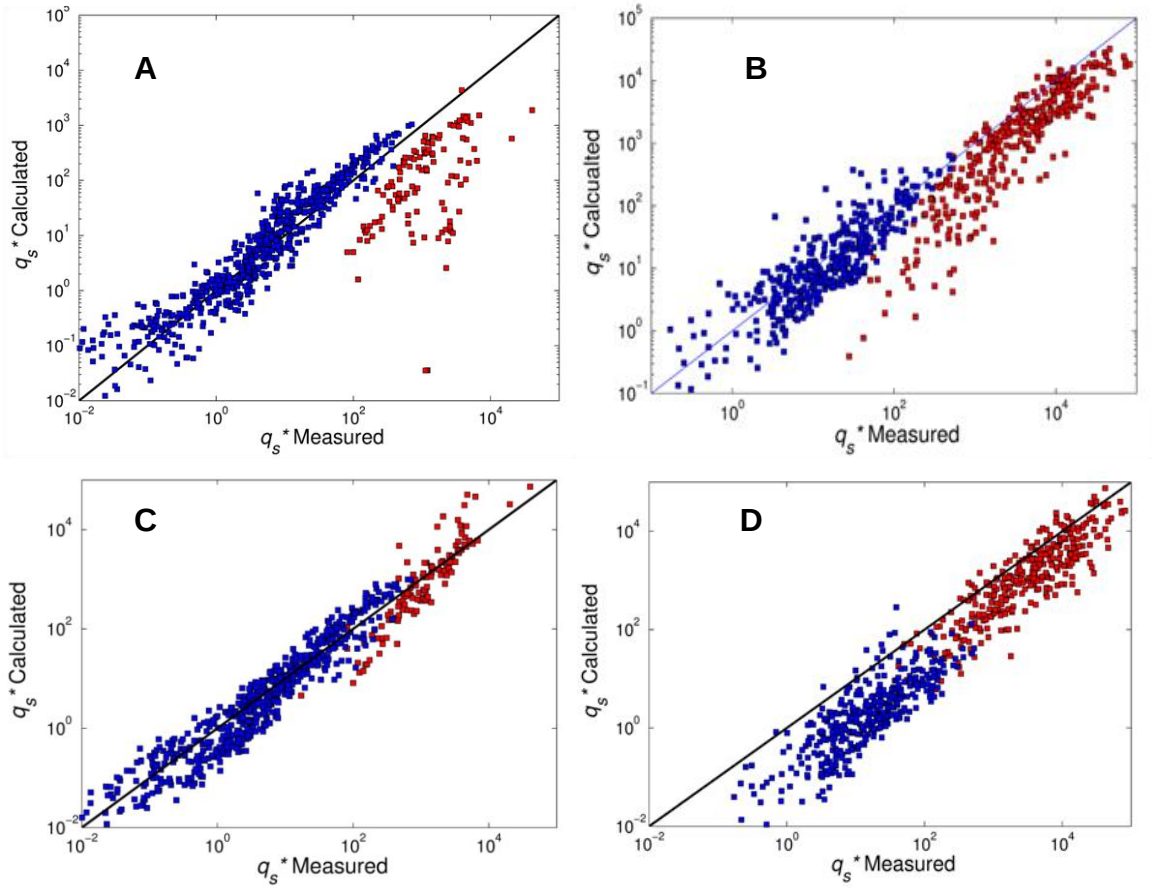

Fig. S6. Performance of two formulae against flume data and field data. The red and blue squares indicate the relative fine- and coarse-grained beds respectively. (*A*-*B*) The van Rijn formula is tested against flume (*A*) and field data (*B*), respectively. (*C*-*D*) The Laursen formula is tested against flume (*C*) and field data (*D*), respectively.

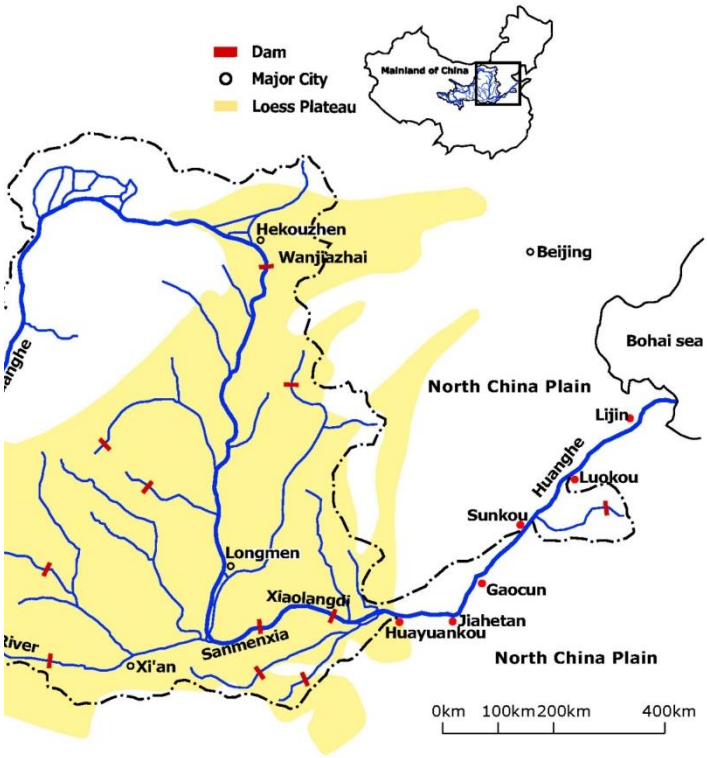

Fig. S7. Map of study areas corresponding to the middle and lower Yellow River, China. Sediment transport data under pre-dam conditions from six major gauging stations are located along the lower Yellow River: Huayuankou, Jiaheyan, Gaocun, Sunkou, Luokou and Lijin respectively. After the construction of Sanmenxia (1958) and Xiaolangdi (1999) dams, the bed material grain size at Huayuankou, the closest gauging station downstream the reservoirs, coarsened significantly. The bed returned to its original fine-grained state during the 1980's.

Movie S1 (separate file). Demonstration of the transition from the high (GEH) to low (EH) efficiency regime of fine-grain transport.

References

1. E. M. Laursen, The total sediment load of streams. *Journal of the Hydraulics Division* **84**, 1-36 (1958).
2. W. R. Brownlie, N. H. Brooks, *Prediction of flow depth and sediment discharge in open channels*. (California Institute of Technology, Pasadena, CA, 1982).
3. J. D. Smith, S. McLean, in *Bottom Turbulence: Proceedings of the 8th International Liege Colloquium on Ocean Hydrodynamics* (eds Nihoul, J.C.J.) **112**, 123–151 (Elsevier, 1977).
4. L. C. van Rijn, Sediment transport, part II: suspended load transport. *Journal of Hydraulic Engineering* **110**, 1613-1641 (1984).
5. P. Diplas *et al.,* The Role of Impulse on the Initiation of Particle Movement Under Turbulent Flow Conditions. *Science* **322**, 717-720 (2008).
6. P. Frey, M. Church, How River Beds Move. *Science* **325**, 1509-1510 (2009).
7. H. Ma *et al.,* Bed load transport over a broad range of timescales: Determination of three regimes of fluctuations. *Journal of Geophysical Research: Earth Surface* **119**, 2653-2673 (2014).
8. J. Heyman, H. B. Ma, F. Mettra, C. Ancey, Spatial correlations in bed load transport: Evidence, importance, and modelling. *Journal of Geophysical Research: Earth Surface*, **119**, 1751-1767 (2014).
9. J. Heyman, F. Mettra, H. B. Ma, C. Ancey, Statistics of bedload transport over steep slopes: Separation of time scales and collective motion. *Geophysical Research Letters* **40**, 128-133, doi:10.1029/2012gl054280 (2013).
10. M. Houssais, C. P. Ortiz, D. J. Durian, D. J. Jerolmack, Onset of sediment transport is a continuous transition driven by fluid shear and granular creep. *Nat Commun* **6**, doi:10.1038/ncomms7527 (2015).
11. M. Houssais, C. P. Ortiz, D. J. Durian, D. J. Jerolmack, Rheology of sediment transported by a laminar flow. *Physical Review E* **94**, 062609 (2016).
12. R. L. Martin, J. F. Kok, Wind-invariant saltation heights imply linear scaling of aeolian saltation flux with shear stress. *Science Advances* **3**, doi:10.1126/sciadv.1602569 (2017).
13. R. A. Bagnold, *An approach to the sediment transport problem from general physics*. (US government printing office, 1966).
14. Y. Niño, M. García, Engelund's analysis of turbulent energy and suspended load. *Journal of Engineering Mechanics* **124**, 480-483 (1998).
15. Y. Niño, F. Lopez, M. Garcia, Threshold for particle entrainment into suspension. *Sedimentology* **50**, 247-263 (2003).
16. M. Houssais, D. J. Jerolmack, Toward a unifying constitutive relation for sediment transport across environments. *Geomorphology* **277**, 251-264 (2017).
17. M. Garcia, G. Parker, Entrainment of Bed Sediment into Suspension. *Journal of Hydraulic Engineering* **117**, 414-435 (1991).
18. S. Wright, G. Parker, Flow resistance and suspended load in sand-bed rivers: simplified stratification model. *Journal of Hydraulic Engineering* **130**, 796-805 (2004).